Identifying the Occurrence Time of the Destructive Kahramanmaraş-Gazientep Earthquake of Magnitude M7.8 in Turkey on 6 February 2023

Sarlis, N. V., Skordas, E. S., Christopoulos, S-R. G. & Varotsos, P. K.

Article

Identifying the Occurrence Time of the Destructive Kahramanmaraş-Gaziantep Earthquake of Magnitude M7.8 in Turkey on 6 February 2023 †

Nicholas V. Sarlis [1,2,*], Efthimios S. Skordas [1,2], Stavros-Richard G. Christopoulos [2,3,4] and Panayiotis K. Varotsos [5]

1 Section of Condensed Matter Physics, Department of Physics, National and Kapodistrian University of Athens, Panepistimiopolis, Zografos, 157 84 Athens, Greece; eskordas@phys.uoa.gr
2 Solid Earth Physics Institute, Department of Physics, National and Kapodistrian University of Athens, Panepistimiopolis, Zografos, 157 84 Athens, Greece; s.r.christopoulos@hud.ac.uk
3 Department of Computer Science, School of Computing and Engineering, University of Huddersfield, Huddersfield HD1 3DH, UK
4 Centre for Computational Science and Mathematical Modelling, Coventry University, Coventry CV1 2TU, UK
5 Department of Operational Informatics and Geospatial Analysis, Division of Informatics and Telecommunications, Hellenic Fire Brigade, 183 46 Athens, Greece; panvar@phys.uoa.gr
* Correspondence: nsarlis@phys.uoa.gr; Tel.: +30-210-727-6735
† To the memory of the Academician Seiya Uyeda.

Abstract: Here, we employ natural time analysis of seismicity together with non-extensive statistical mechanics aiming at shortening the occurrence time window of the Kahramanmaraş-Gaziantep M7.8 earthquake. The results obtained are in the positive direction pointing to the fact that after 3 February 2023 at 11:05:58 UTC, a strong earthquake was imminent. Natural time analysis also reveals a minimum fluctuation of the order parameter of seismicity almost three and a half months before the M7.8 earthquake, pointing to the initiation of seismic electrical activity. Moreover, before this earthquake occurrence, the detrended fluctuation analysis of the earthquake magnitude time-series reveals random behavior. Finally, when applying earthquake nowcasting, we find average earthquake potential score values which are compatible with those previously observed before strong ($M \geq 7.1$) earthquakes. The results obtained may improve our understanding of the physics of crustal phenomena that lead to strong earthquakes.

Keywords: earthquakes; natural time; time-series; entropy; criticality; complex systems

1. Introduction

The Kahramanmaraş-Gaziantep M_w7.8 Pazarcik earthquake (EQ) [1] took place on 6 February 2023 at 01:17:35 UTC and was followed within 9 h by the M_w7.5 Elbistan EQ [2] at 10:24:48 UTC, giving rise to the 2023 Kahramanmaraş, Turkey, EQ doublet [3]; see Figure 1. According to the International Blue Crescent Relief and Development Foundation [4] situation report, the Turkish Ministry of Interior had announced that the fatal casualties in the Kahramanmaraş EQs doublet totaled more than 50,399 lives. Moreover, 8476 people lost their lives in Syria, which was also affected by these EQs. It was one of the deadliest disasters in Turkey and Syria during the last millennium [3]. In total, 16 percent of Turkey's population, that is 14 million people, were affected by these catastrophic events [4].

Almost two weeks before the Kahramanmaraş EQ doublet, i.e., on 25 January 2023, a paper was submitted [5] in which a novel procedure for estimating the time of occurrence of an impending strong EQ was presented. This new procedure was based on the combination of the results obtained from natural time analysis (NTA), see below, and non-extensive

statistical mechanics (NESM) pioneered by Tsallis [6]. Tsallis [6] introduced a new functional form for the entropy, which is now generally called Tsallis entropy [7–16]

$$S_q = k_B \frac{\left(1 - \sum_i p_i^q\right)}{(q-1)}, \tag{1}$$

where $q \in \mathcal{R}$ is the entropic index, $\{p_i\}$ are the probabilities for each microstate i and k_B is the Boltzmann constant. In the case $q \to 1$, Equation (1) recovers the Boltzmann entropy

$$S_B = -k_B \sum_i p_i \ln p_i. \tag{2}$$

Using a fragment–asperity model [17], Posadas and Sotolongo-Costa [18] have recently estimated the Tsallis entropy S_q for the case of EQs; for further details, see Section 2.4. It is the combination of the latter quantity with the entropy change ΔS under time reversal in NTA that allows the estimation of the occurrence time of the impending EQ [5].
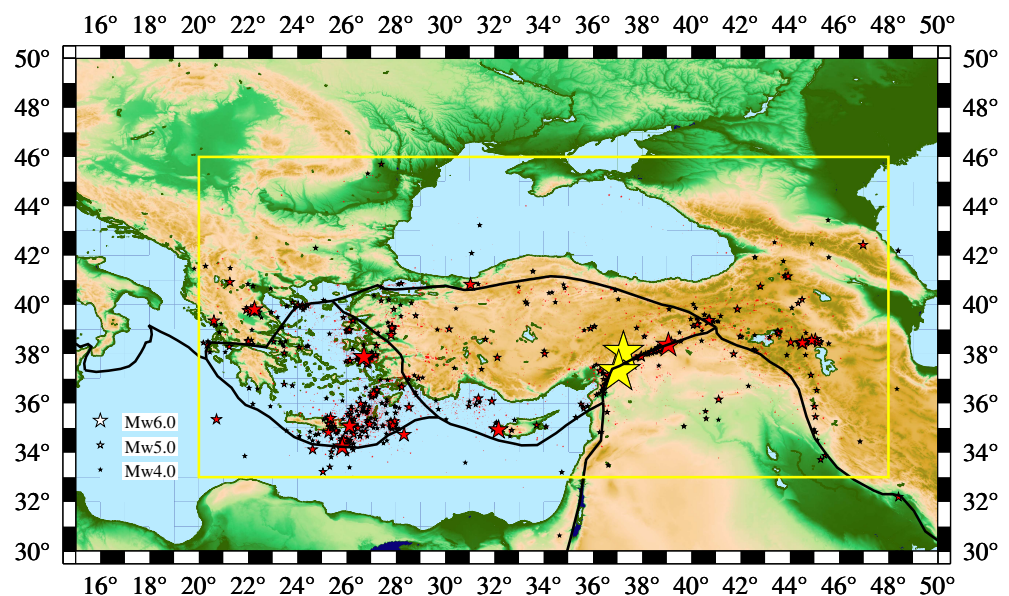
Figure 1. The epicenters (red stars) of all EQs reported by AFAD with magnitude $M \geq 2.0$ during the period 1 January 2020 to 31 December 2022 (see Section 2.1). The yellow stars depict the epicenters of the Kahramanmaraş-Gaziantep $M_w 7.8$ Pazarcik EQ [1] and the $M_w 7.5$ Elbistan EQ [2] that occurred on 6 February 2023 at 01:17:34 UTC and 10:24:48 UTC, respectively. The black thick lines depict the tectonic plate boundaries [19].

NTA, which is based on a new concept of time termed natural time, was introduced in 2001 [20] and has found useful applications that range from EQ preparatory processes to heart dynamics [21–32] and from atmospheric sciences [33–36] to finance [37]; for a recent review, see [38]. It was originally focused on the discrimination of the low-frequency ($f \leq 1$ Hz) electric signals that are observed before EQs, which are called Seismic Electric Signals (SES) [23,39–53], from similar-looking signals of man-made origin [54]. The physical properties of SES [23,42] provide information on the magnitude M of the impending EQ, on the probable epicentral area, and an estimation of its occurrence time. In the first publications by Varotsos et al. [20,54], it was shown that NTA may reveal that SES exhibited critical dynamics, while it has been also used for the identification of criticality in the seismicity inside the probable epicentral area. As will be further elaborated in Section 2.3, NTA there may provide a first estimate of the occurrence time of the impending EQ [20,44,55,56] (see also Chapter 7 of [23] and Chapters 5 and 9 of [38]). Additionally, NTA provides means to identify temporal correlations between EQ magnitudes (see Section 6.3 of [23] and references therein), which is a very hot topic, see, e.g., the recent meta-analysis by Petrillo

and Zhuang [57]. Within the NTA framework, an entropy *S* has been introduced [20,54]; see Section 2.3 for its detailed properties. Most importantly, *S* has found useful applications in seismicity as well as in a variety of other physical systems, see, e.g., Chapters 7, 8, 9, and 13 of [38]. Earthquake nowcasting [58–66], which enables seismic hazard estimation, is also based on natural time; see Section 2.6. As Rundle et al. [58] state, natural time when applied to EQ seismicity has the advantage that it is not necessary to decluster the aftershocks.

It is important to note, however, that the study of the time-occurrence series of EQs may provide additional information to that obtained by NTA. The fractal and multifractal character of such time-series has been studied by Telesca et al. [67] and Telesca and Lapenna [68], revealing new properties of seismicity. Recently, the fractal characteristics of seismicity identified by the interevent times have found useful applications to cases of induced seismicity [69], see also [70], as well as in the case of the Anatolian region with implications for seismic hazards before and during the 2023 Kahramanmaraş seismic sequence [71]. Additionally, in forecasting fractal studies, see, e.g., [72,73], declustered catalogs are used. To date, NTA has not been applied to such catalogs. Such an application, however, may lead to interesting results and is within the future plans of our group.

So far, the new procedure introduced by Varotsos et al. [5] has been applied to the case of the super-giant 2011 *M*9 Tohoku EQ in Japan as well as in three strong EQs in the western part of northern America [74], which included the 2017 *M*8.2 Chiapas Mexico EQ, the deadly 19 September 2017 *M*7.1 Mexican flatslab EQ, and the 2019 Ridgecrest *M*7.1 EQ in California. It is the purpose of the present paper to examine whether this procedure could have been applied before the Kahramanmaraş-Gaziantep M_w7.8 Pazarcik EQ in order to provide an improved estimate of the EQ occurrence compared to that previously found solely by means of NTA [20,51,75–77]. The paper is organized as follows. In Section 2, the EQ catalog and the methods used are presented, the results are shown and discussed in Section 3, and our conclusions are summarized in Section 4.

2. Materials and Methods
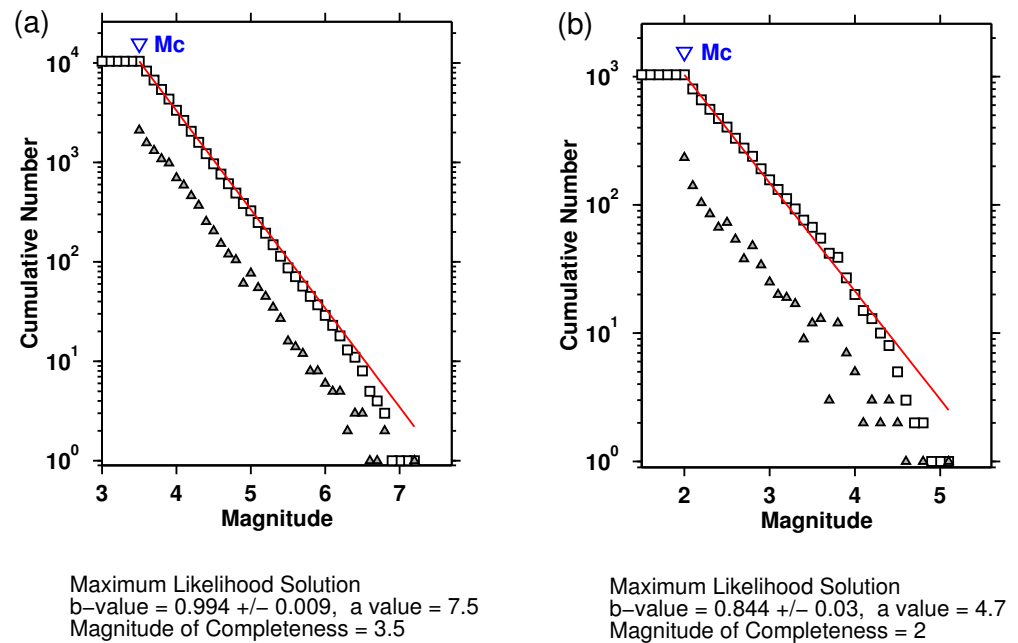
2.1. The Seismic Data Used

The seismic data used come from the Turkish Disaster and Emergency Management Authority (AFAD) and are publicly available at the site https://deprem.afad.gov.tr/event-catalog (last accessed on 7 May 2023). We considered all EQs within the region $N_{33}^{46}E_{20}^{48}$ (see the yellow rectangle in Figure 1).

The frequency–magnitude distribution (FMD) for the EQs during the period 1 January 2002 to 31 December 2022 is shown in Figure 2a, the reported magnitude in 93% of these cases is the local magnitude ML; otherwise, moment magnitude M_w was reported; see https://deprem.afad.gov.tr/event-catalog (last accessed on 7 May 2023). For AFAD, it is reported that ML and M_w scales are almost equivalent for a wide range of magnitude values (see [78] and references therein); thus, this catalog could be considered homogeneous with respect to magnitude (cf. a unified EQ catalog is necessary for this kind of analysis, see, e.g., [79]). There, beyond the cumulative FMD depicted by open squares, the non-cumulative FMD [80] is also shown with open triangles. According to the Gutenberg–Richter (GR) law [81] for EQs, the number of EQs $N(M > m)$ of magnitude (*M*) greater than *m* follows an exponential decay

$$N(M > m) = 10^{a-bm}, \tag{3}$$

where *a* reflects the total rate of sesmicity in the region and the *b*-value (which is usually close to unity, see, e.g., [23]) is related to the level of seismicity in the region (c.f. for a possible correlation between these two parameters see [82]). As shown in Figure 2a (obtained by the standard code ZMAP [83] using maximum likelihood estimation, see, e.g., [84]), the GR law of Equation (3) is valid for $M \geq M_c$, where the magnitude of completeness M_c equals 3.5. We also examined that setting M_c to the latter value, $m = 3.5$, secures temporal completeness since 1 January 2002; see Section 3 below. For the readers' better information, we note that new methods for the estimation of the magnitude distribution parameters

have been recently proposed in the literature [85,86]. Moreover, further details on the seismicity of Turkey and its monitoring can be found in [71] and references therein. Since it will be needed later for the analyses presented in Section 3, we also investigated in Figure 2b the completeness of the catalog obtained from AFAD during the period from 1 January 2020 to 1 January 2023 within a $3° \times 3°$ area centered at the actual epicenter of the Kahramanmaraş-Gaziantep M_w7.8 Pazarcik EQ.

Maximum Likelihood Solution
b–value = 0.994 +/– 0.009, a value = 7.5
Magnitude of Completeness = 3.5

Maximum Likelihood Solution
b–value = 0.844 +/– 0.03, a value = 4.7
Magnitude of Completeness = 2

Figure 2. Cumulative (squares) and non-cumulative (triangles) FMD for the EQs (**a**) within the region $N^{46}_{33}E^{48}_{20}$ during the period 1 January 2002 to 31 December 2022 and (**b**) within a $3° \times 3°$ area centered at the actual epicenter of the Kahramanmaraş-Gaziantep M_w7.8 Pazarcik EQ during the period from 1 January 2020 to 1 January 2023, as estimated by ZMAP [83]. The b-value and M_c have been calculated by applying the maximum curvature method (see, e.g., [87] and references therein) in the automatic selection of ZMAP. The red lines represent the GR relation.

2.2. Seismotectonic Background

The epicenter of the M_w 7.8 EQ is located at the East Anatolian Fault (EAF) zone; see Figure 3. The EAF structure is considered to be a left-lateral strike–slip fault, of ∼700 km length [88], bounding the northeast Arabian plate movement with respect to the Anatolian plate. For the fault segments at the eastern end of the fault zone, this movement occurs at ∼10 mm/yr [88]. At the northeastern part, the left-lateral EAF intersects with the right-lateral North Anatolian Fault (NAF), which are considered to be the main structures in the tectonics of the eastern Mediterranean [89]. The Anatolian microplate is located between EAF and NAF and moves westward under the influence of internal deformation due to the collision of the Arabian and African plates with the Eurasian plate [90]. It is still debated, however, up to what point the EAF is extended to the west [88]. According to Medvedeva et al. [89], the southwestern end of the EAF zone transfers into the Cyprus Island Arc and the Dead Sea Fault zone. The focal mechanism solution for the M_w 7.8 EQ indicates a left-lateral strike–slip with a length of the ruptured fault zone ∼300 km (see Ref. [89] and references therein).
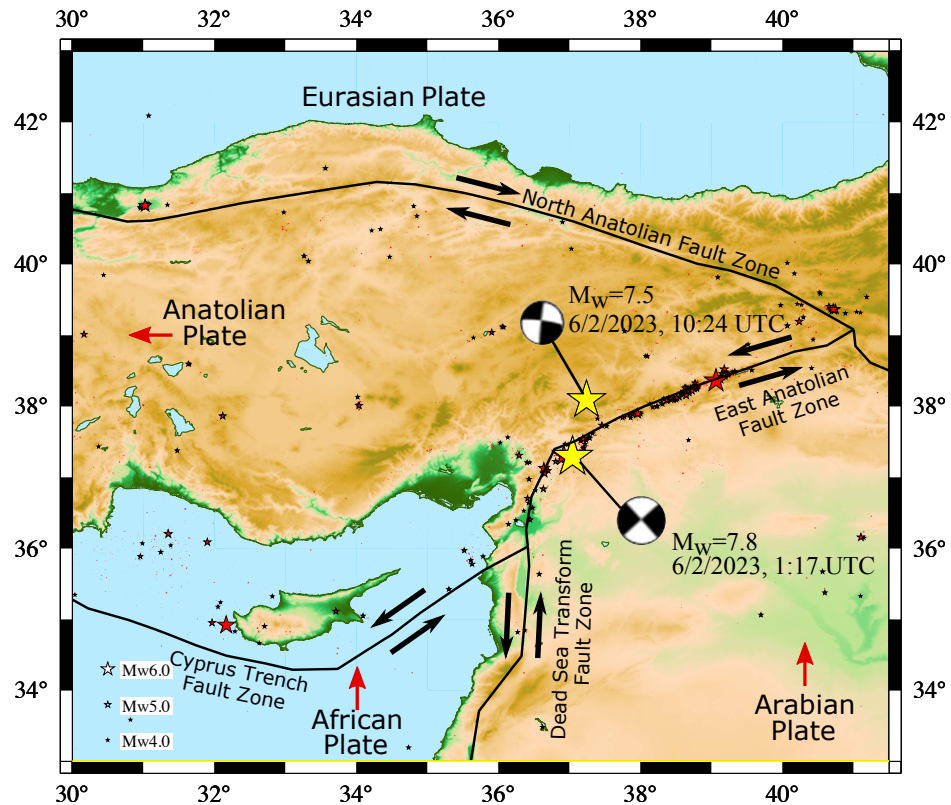
Figure 3. The tectonic settings of the Anatolian region along with the epicenters (yellow stars) and the focal mechanisms of the two catastrophic EQs of $M_w = 7.8$ at 01:17:34 UTC and $M_w = 7.5$ at 10:24:48 UTC on 6 February 2023. The red arrows indicate the movement of the tectonic plates, and the black arrows indicate the direction of movement along the major fault zones; see [89] and references therein (cf. for a review of the historical seismicity in the region, see [91]).

2.3. Natural Time Analysis: Background

In a series comprising N EQ events (which can be considered as a temporal point pattern [5,92]), natural time χ_k corresponding to the k-th EQ of magnitude M_k is defined [20] as $\chi_k = k/N$. Thus, we abandon the notion of conventional time but maintain the EQ energy Q_k ($\propto 10^{1.5M_k}$, see, e.g., [93] and Chapter 6 of [23]) together with the order of occurrence k. In NTA, the pair (χ_k, p_k), where $p_k = Q_k / \sum_{n=1}^N Q_n$ is the normalized energy, is attributed to each event k, and we consider the normalized power spectrum $\Pi(\omega) \equiv |\Phi(\omega)|^2$, where $\Phi(\omega) = \sum_{k=1}^N p_k \exp(i\omega\chi_k)$. The quantities p_k can be considered (see, e.g., Appendix A.3 of [38] and references therein) as probabilities, and hence $\Phi(\omega)$ with $\omega \in \mathcal{R}$ corresponds to the characteristic function [94] for p_k. This characteristic function provides information for the distribution: for example, the moments $\langle \chi^m \rangle = \sum_{k=1}^N \chi_k^m p_k$ that are equal to the derivatives $d^m\Phi(\omega)/d\omega^m$ ($m > 0$) at $\omega \to 0$. In a similar sense, when considering $\Pi(\omega)$ in the region of ω close to 0, a quantity κ_1 was obtained from the Maclaurin series

$$\Pi(\omega) = 1 - \kappa_1\omega^2 + \kappa_2\omega^4 + \dots, \tag{4}$$

where

$$\kappa_1 = \langle \chi^2 \rangle - \langle \chi \rangle^2 = \sum_{k=1}^N p_k(\chi_k)^2 - \left(\sum_{k=1}^N p_k\chi_k \right)^2. \tag{5}$$

For the case of SES activities, mentioned in the Introduction, that exhibit critical dynamics [54], it has been shown [20,23] that the corresponding $\Pi(\omega)$ takes the form:

$$\Pi_{crit}(\omega) = \frac{18}{5\omega^2} - \frac{6\cos\omega}{5\omega^2} - \frac{12\sin\omega}{5\omega^3}. \tag{6}$$

Moreover, it has been shown that

$$\kappa_1 \approx 0.070 \tag{7}$$

at criticality for various dynamical systems [20,23,38,95] that include SES activities; see, e.g., Table 8.1 on page 343 of [23]. In general, κ_1 is suitable for identifying the approach to a critical point. Especially, in NTA of EQs, κ_1 can be thought of [23,38] as an order parameter (OP) for seismicity because its value diminishes abruptly when a strong EQ takes place, while the statistics of its fluctuations share properties observed in well-known critical systems [96].

One of the advantages of NTA is that it allows for monitoring the fluctuations of the OP of seismicity within an EQ catalog. For this purpose, we consider an excerpt of this catalog consisting of W successive events. We then deduce the totality of κ_1 values resulting from subexcerpts of the successive 6 to W EQs. For this set of κ_1 values, we calculate the mean value $\mu(\kappa_1)$ and the standard deviation $\sigma(\kappa_1)$, leading to the variability of κ_1:

$$\beta_W = \frac{\sigma(\kappa_1)}{\mu(\kappa_1)} \tag{8}$$

that quantifies the κ_1 fluctuations within this EQ catalog excerpt. The quantity β_W of Equation (8) is interrelated with the square root of the Ginzburg criterion (cf. Equation (6.25) of [97]) whose usefulness in the physics of EQs has been explained by Holliday et al. [98]. Finally, how β_W varies in conventional time can be pursued by sliding event by event the window of W consecutive EQs in the EQ catalog; the occurrence time of the EQ that followed the last one of the window studied is attributed to each β_W obtained. It has been experimentally observed that appropriately selected minima of β_W labeled $\beta_{W,min}$ in regional EQ catalogs [51,99] coincide with the initiation of the emission of SES activities signaling that a strong EQ is going to occur within a maximum lead time of $5\frac{1}{2}$ months [23].

The entropy S in natural time [20,54] is given by

$$S = \langle \chi \ln \chi \rangle - \langle \chi \rangle \ln \langle \chi \rangle = \sum_{k=1}^{N} p_k \frac{k}{N} \ln\left(\frac{k}{N}\right) - \left(\sum_{k=1}^{N} p_k \frac{k}{N}\right) \ln\left(\sum_{k=1}^{N} p_k \frac{k}{N}\right). \tag{9}$$

In the case of a "uniform" distribution [54], Q_k are considered independent and identically distributed (IID) positive random variables and S becomes $S_u \equiv \frac{\ln 2}{2} - \frac{1}{4} \approx 0.0966$. The application [23,38] of time-reversal $\hat{T}$, i.e., $\hat{T} p_k = p_{N-k+1}$, in Equation (9) leads to

$$S_- = \sum_{k=1}^{N} p_{N-k+1} \frac{k}{N} \ln\left(\frac{k}{N}\right) - \left(\sum_{k=1}^{N} p_{N-k+1} \frac{k}{N}\right) \ln\left(\sum_{k=1}^{N} p_{N-k+1} \frac{k}{N}\right). \tag{10}$$

The quantity S_- differs from S, leading to an entropy change

$$\Delta S \equiv S - S_- \tag{11}$$

upon time reversal. Thus, S is time-reversal asymmetric [23]. Moreover, S is a *dynamic* entropy, different from static ones, e.g., Shannon entropy, that is positive, concave, and experimentally (Lesche) stable [100,101] (see Chapter 3 of [23]).

The entropy change ΔS under time reversal is also crucial for the identification of the approach of the system to a dynamic phase transition [5,38,74]. For this purpose, S and S_- are calculated for a natural time window of length i (=number of consecutive events) sliding event by event through the whole time-series. Equation (11) is then used for estimating ΔS, thus resulting in a time-series of consecutive ΔS_i values.

NTA can provide an estimate of the occurrence time of the impending EQ when analyzing seismicity in the area candidate to suffer the strong EQ after the initiation of an SES activity or after the observation of $\beta_{W,min}$. Such examples for Greece can be found in

Chapter 7 of [23] while for Japan, Mexico, and California, they can be found in Chapter 5 of [38]. Usually [20,22,44,55,56], the strong EQ occurs a few days up to one week or so after a true coincidence of $\Pi(\omega)$ of the evolving seismicity to that of the critical state, $\Pi_{crit}(\omega)$ of Equation (6). The following criteria have been used (see, e.g., [23,38]) to assure such a coincidence:

1. The "average" distance $\langle D \rangle$ between the curves of $\Pi(\omega)$ and $\Pi_{crit}(\omega)$ for $\omega \leq \pi$ should be $\langle D \rangle < 10^{-2}$. Details on this calculation can be found in [20,23].
2. The final approach of the evolving $\Pi(\omega)$ to $\Pi_{crit}(\omega)$ must be from below, see, e.g., Figure 5 of [77], which alternatively means that κ_1 gradually decreases with time before reaching the critical value 0.070 of Equation (7).
3. At the coincidence, both entropies S and S_- in natural time must be smaller than S_u.
4. Since this process (critical dynamics) is considered to be self-similar, the occurrence time of the true coincidence should not markedly vary upon changing the magnitude threshold M_{thres} which is used for NTA of seismicity.
5. The final approach described by the second criterion starts to be obeyed after an EQ for which ΔS of seismicity in the candidate epicentral area under time reversal exhibits a local minimum. In simple words, after S_- exceeds S by a large amount, κ_1 starts decreasing to finally approach 0.070.

2.4. Non-Extensive Statistical Mechanics Model for EQs

Sotolongo-Costa and Posadas [17] introduced a fragment–asperity model for EQs which is based on NESM. They considered two rough surfaces, the movement of which is hindered by fragments. The latter are generated during EQ occurrence by breakage of the plates simulating the fault. The magnitude of an EQ is related to distribution of the fragment sizes which effectively determine the value of the stress needed to overcome asperities and allow motion of the plates. Hence, the EQ energy is related to the size of the fragments, the distribution of which is determined by maximizing the Tsallis entropy of Equation (1). The model was later revisited by Silva et al. [10] by employing a more realistic relation between EQ energy and the size of the fragments. Most interestingly, the NESM model of EQs provided a generalization of the GR law for the distribution of EQ magnitudes, which relates [12,14] the aforementioned (see Section 2.1) *b*-value with the non-extensivity parameter *q* according to the formula

$$b = 2\frac{(2-q)}{(q-1)}. \tag{12}$$

Posadas and Sotolongo-Costa [18] extended this study significantly by directly estimating the Tsallis entropy S_q of the fragments. Thus, the GR distribution for EQs by means of Equation (12) is now related to a well-defined value

$$S_q = \frac{\left[1 - (2-q)^{\frac{1}{(2-q)}}\right]}{(q-1)}, \tag{13}$$

where the Boltzmann constant k_B in Equation (1) was set to unity.

2.5. Detrended Fluctuation Analysis of EQ Magnitudes

Detrendred fluctuation analysis (DFA) was firstly introduced by Peng et al. [102] as a method for the quantification of long-range correlations in non-stationary time-series. A comparison of DFA with power spectral methods and wavelet-based estimators of scaling behavior can be found in [103,104], respectively. DFA has found useful applications in a wide variety of fields ranging from the study of DNA [102,105,106] and biological signals [107–111] to EQs [112], meteorology [113,114] and atmospheric physics [115]. DFA has been generalized into a multifractal method by Kantelhardt et al. [116] which has also found widespread applications, see, e.g., [117–119], including seismicity.

In the case of DFA of EQ magnitudes, we first sum the time-series of consecutive EQ magnitudes $\{M_k\}_{k=1,2,\dots,W}$ to obtain the profile $y_m = \sum_{k=1}^{m}(M_k - \langle M \rangle)$ after removing the average value $\langle M \rangle = \sum_{k=1}^{W} M_k / W$. Then, we divide the W values of the profile into l equal non-overlapping segments and find the polynomial of order n trend $y_n(m)$ in each segment. The root mean square fluctuation is defined as the DFA measure

$$F_{DFA}(s) = \sqrt{\sum_{m=1}^{W} \frac{[y_m - y_n(m)]^2}{W}} \qquad (14)$$

at scale $s = W/l$. We repeat this procedure for various values of l and examine the validity of the scaling relation $F_{DFA}(s) \propto s^a$, where the exponent a is called the DFA exponent. This exponent characterizes the correlation properties of the EQ magnitude time-series: when $a < 0.5$, $\{M_k\}_{k=1,2,\dots,W}$ is anti-correlated, if $a \approx 0.5$, the time-series is not correlated (white noise), while $a > 0.5$ indicates the presence of long-range correlations. In the present application, we used a window of $W = 300$ consecutive EQ magnitudes moving by one EQ each time along the AFAD EQ magnitude time-series to obtain a new time-series of a_{300}. For the calculation of the DFA exponents a_{300}, we employed the DFA [102,120] computer program `dfa.c` of Physionet [121] (it is freely available at https://www.physionet.org/content/dfa/1.0.0/dfa.c, last accessed on 19 May 2023).

2.6. Earthquake Nowcasting

Using the concept of natural time, Rundle et al. [58] introduced EQ nowcasting to estimate seismic hazards [29,32,59,65,66,122–130]. Many applications of EQ nowcasting have been published in various fields of Earth Sciences including induced seismicity [60,62], the temporal clustering of EQs [61], and theoretical EQ models [131], while recently the method has been applied [132] for nowcasting volcanic eruptions.

Our group in a series of publications [124,125,129] has employed EQ nowcasting to obtain epicentral information for a future EQ. To this end, the EQ potential score (EPS) of EQ nowcasting is calculated [58] using the cumulative distribution function $F(n_s)$ for the number n_s of 'small' EQs (of magnitude $M \geq M_\sigma$) that take place in the time interval between two 'large' EQs (of magnitude $M \geq M_\lambda$) within a large region, e.g., $N_{23}^{52}E_5^{50}$ for the eastern Mediterranean [124]. Using a self-consistency radius R, Varotsos et al. [124] introduced average EPS maps by calculating n_s within a circle of radius R centered at a point (x_{ij}, y_{ij}) of a square lattice—denoted by $(n_s)_{ij}$— and averaged the resulting EPS values $F[(n_s)_{ij}]$ within the same radius R to obtain at a point $(x_{i_0j_0}, y_{i_0j_0})$ the value

$$\langle \text{EPS} \rangle \equiv \frac{1}{N} \sum_{i,j}^{d(x_{i_0j_0}, y_{i_0j_0}; x_{ij}, y_{ij}) \leq R} F[(n_s)_{ij}], \qquad (15)$$

where the summation is restricted to the lattice points whose distance $d(x_{i_0j_0}, y_{i_0j_0}; x_{ij}, y_{ij})$ from the observation point $(x_{i_0j_0}, y_{i_0j_0})$ is smaller than or equal to R, and N stands for the number of these points. The study of the eastern Mediterranean which is relevant to our case of the Kahramanmaraş, Turkey, EQ doublet [3] resulted in an optimum value of $R = 250$ km when using $M_\sigma = 4.0$, $M_\lambda = 6.0$ leading to

$$F(n_s) = 1 - \exp\left[-\left(\frac{n_s}{134.9}\right)^{0.973}\right], \qquad (16)$$

when using the United States National Earthquake Information Center Preliminary Determination of Epicenter (US-NEIC PDE) catalog available from the United States Geological Survey https://earthquake.usgs.gov/earthquakes/search/ (last accessed on 19 May 2023); for more details, see [124].

3. Results and Discussion

The results shown in Figure 2a, together with the fact that the variability β_W of the OP of seismicity when using local EQ catalogs in various regions of the world [74,77,133] has been made for $M \geq M_{thres}$ with $M_{thres} = 3.5$, led us to select for such an analysis in natural time only the EQs with $M \geq 3.5$. Upon this selection, we have that the average rate of EQs (of $M \geq 3.5$) within $N_{33}^{46}E_{20}^{48}$ is around 50 EQs per month. By employing the method of analysis presented in Section 2.3, we found for β_W with W = 300, 250, 200, 150, and 100, which correspond to time periods of six to two months practically covering the aforementioned lead time of SES activities, the results shown in Figure 4.

In this figure, we present β_W during the almost 20-year period 1 January 2002 to the time of occurrence of the Kahramanmaraş, Turkey, EQ doublet on 6 February 2023. In Figure 4e, we present in an expanded time scale the results during the final period from 1 January 2022 to 6 February 2023. Although β_W for different values of W exhibit different dynamics, we observe that *all* β_W values studied exhibit local minima during the period from 14 August 2022 to 18 October 2022 whose values lie between $\beta_{300,min} = 0.319$ and $\beta_{200,min} = 0.297$. The ratio $\beta_{300,min}/\beta_{200,min} \approx 1.07$ falls within the limits found [133] in Japan for the variability minima that preceded all EQs of magnitude $M \geq 7.6$ since 1984 (cf. this criterion was also found valid; see, e.g., Section 1.5.1 of [38], for the case of the 2015 $M_w 7.9$ Ogasawara EQ, which is the single $M \geq 7.6$ EQ in Japan after the $M9$ Tohoku EQ studied in [133]).

As stated in the Appendix of [134], for a variability minimum to be of precursory nature, the EQs that lead to the minima $\beta_{200,min}$ and $\beta_{300,min}$ should belong to the same *critical* process before the strong EQ. This fact was secured [134] by inspecting whether 90% of the EQs that led to $\beta_{200,min}$ are included in the EQs that led to $\beta_{300,min}$. Turning now to the present case, we examine whether such a critical process is also observed in the present case. For this reason, we inspect from the EQ catalog whether the EQs that lead to a minimum, e.g., $\beta_{100,min}$, are included in the EQs leading to $\beta_{150,min}$ or $\beta_{200,min}$ or $\beta_{250,min}$ or $\beta_{300,min}$. We found that in all combinations $W' < W$, the EQs that lead to $\beta_{W',min}$ of Figure 4e are included in the EQs that lead to $\beta_{W,min}$ with percentages that exceed 98%. Hence, according to [134], the variability minima of Figure 4e belong to the same critical process that preceded by almost three and a half months (when considering the time lag Δt_{300} since $\beta_{300,min}$) the Kahramanmaraş, Turkey, EQ doublet.

An inspection of Figure 4 reveals that such a critical process leading to simultaneous (within almost two months, i.e., 14 August to 18 October 2022) minima of β_W within the aforementioned limits $[0.297, 0.319]$ is unique during the almost 20-year period of our study that consists of 241 months. Hence, the probability of observing by chance such a phenomenon could be approximated by $2/241 \approx 1.2\%$, which points to the statistical significance of the critical process identified in Figure 4e.

Here, we note that NTA focuses on the identification of precursory behavior before strong EQs. An inspection of Figure 4 reveals that during the study period from 1 January 2002 to the time of occurrence of the Kahramanmaraş-Gaziantep $M_w 7.8$ Pazarcik EQ, the only EQ with $M > 7.0$ that occured in the region is the $M_w 7.3$ Halabaya EQ on 12 November 2017 [135]; see Figure 4d. This EQ has been shown to result in a variability minimum when studying the seismicity in a wider area, i.e., that of the eastern Mediterranean [136], in conjunction with EQ networks based on similar activity patterns [137]. The exact details of the corresponding variability minimum can be found in Table 3 and Figure 4b of [136]. The statistical significance and the predictive ability of the precursory β_W minima have been discussed in detail in Sections 1.5.2, 12.13.1 and 12.13.2 of [38] by employing receiver operating characteristics [138] as well as event coincidence analysis [139,140]. For EQs of magnitude $M < 7.0$, NTA has to be combined with the preseismic information carried by SES, see, e.g., [23,44,55,56], in order to provide an improved estimation of the occurrence time of the impending EQ.

The fact that this critical process is of a truly precursory nature is also strengthened because the behavior of the DFA exponent a_{300} is compatible with that previously found in

Japan [134] (see their Figures 3–8), Mexico [75] (see their Figure 3), and California [76] (see their Figure 3). In Figure 4e, we observe that during the period when the minimum was observed, values of a_{300} well above 0.5 appear, pointing to long-range correlations (cf. on 15 September 2022 $a_{300} = 0.62$), while later and just before the Kahramanmaraş, Turkey, EQ doublet, a_{300} fluctuates around 0.5, indicating a breakdown of the correlations to a random behavior (cf. on 19 January 2022 $a_{300} = 0.46$).
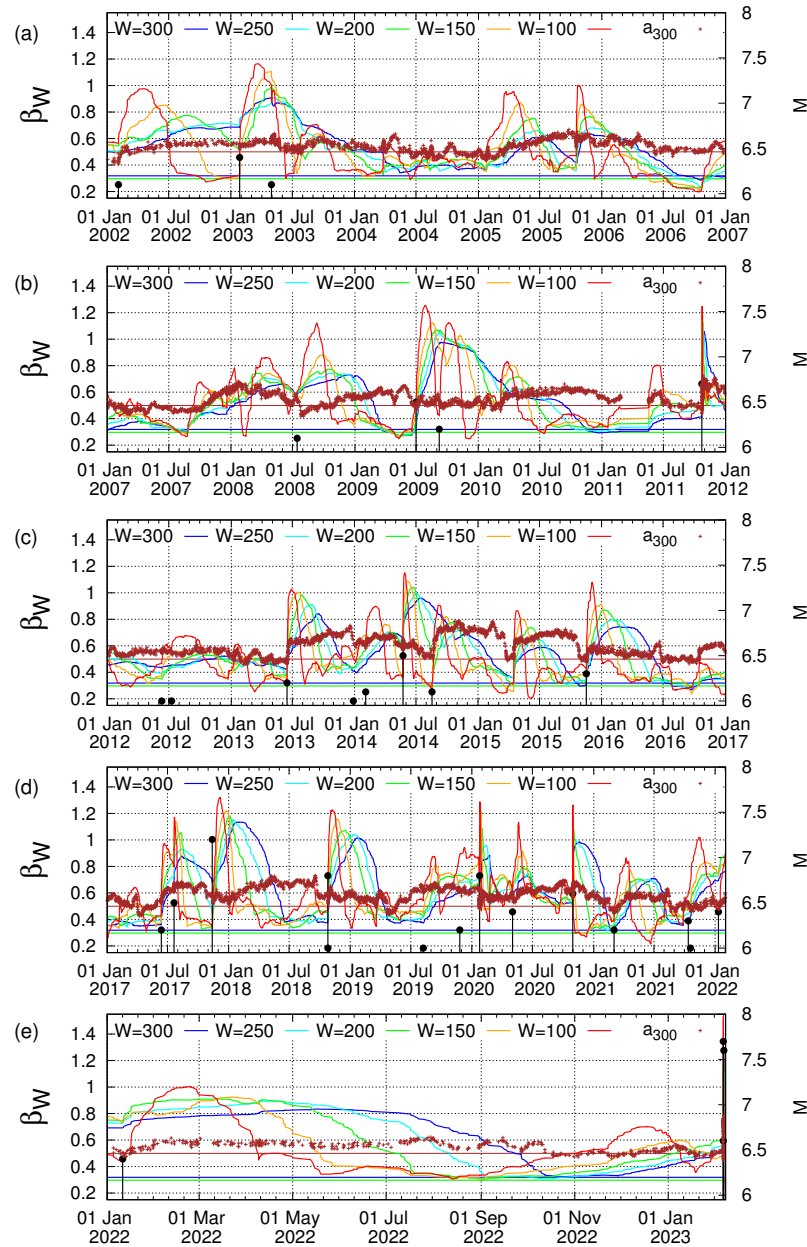
Figure 4. The variabilities β_W (left scale) for $W = 300$ (blue), 250 (cyan), 200 (green), 150 (orange), and 100 (red), versus the conventional time since 1 January 2002 until the Kahramanmaraş, Turkey, EQ doublet. Panels (**a–e**) correspond to consecutive time periods. The brown plus symbols depict the values of the DFA exponent a_{300} (left scale) estimated within a moving window of 300 consecutive EQs; see Section 2.5. The brown horizontal line corresponds to $a_{300} = 0.5$. The blue and green horizontal lines correspond to $\beta_{300,min}$ and $\beta_{200,min}$, respectively, that border the $\beta_{W,min}$ for $W = 300$, 250, 200, 150, and 100 observed during the period 14 August 2022 to 18 October 2022 before the Kahramanmaraş-Gaziantep M_w7.8 Pazarcik EQ; see panel (**e**). The EQs reported by AFAD are shown with the black candlesticks ending at circles, the magnitude M of which can be read using the right scale.

The observation of a precursory variability minimum is expected [48,51,75,76,99] to be accompanied by the initiation of an SES activity. The occurrence time of the impending EQ can be estimated by analyzing the seismicity in the area probable to suffering from strong EQs in order to identify the fulfillment of the five criteria mentioned in Section 2.3. In the present case of the Kahramanmaraş-Gaziantep $M_w7.8$ Pazarcik EQ, however, no SES data were available, since a Varotsos–Alexopoulos–Nomicos (VAN) telemetric network [23,40–43] does not operate in Turkey [53]. Thus, such an estimation of the area to suffer from strong EQs by means of SES is missing. To overcome this difficulty and in order to examine whether seismicity has reached criticality in the epicentral region, we decided—in this a posteriori study—to investigate the seismicity after 18 October 2022 within a $3° \times 3°$ area centered at the actual epicenter of the Kahramanmaraş-Gaziantep $M_w7.8$ Pazarcik EQ. An NTA of seismicity was made for various magnitude thresholds $M_{thres} = 2.0, 2.1, \ldots 3.2$ and the five criteria of Section 2.3 were found to be obeyed in all the 13 cases examined, while for eight of them, the date of true coincidence was observed from 17 to 21 January 2023, i.e., almost two weeks before the Kahramanmaraş, Turkey, EQ doublet. Indicative results of such a study are shown in Figure 5. This two-week time lag would have been the estimation of the occurrence time of the Kahramanmaraş-Gaziantep $M_w7.8$ Pazarcik EQ by means of NTA if we did not proceed to the combination of NTA with NESM in [5,74].
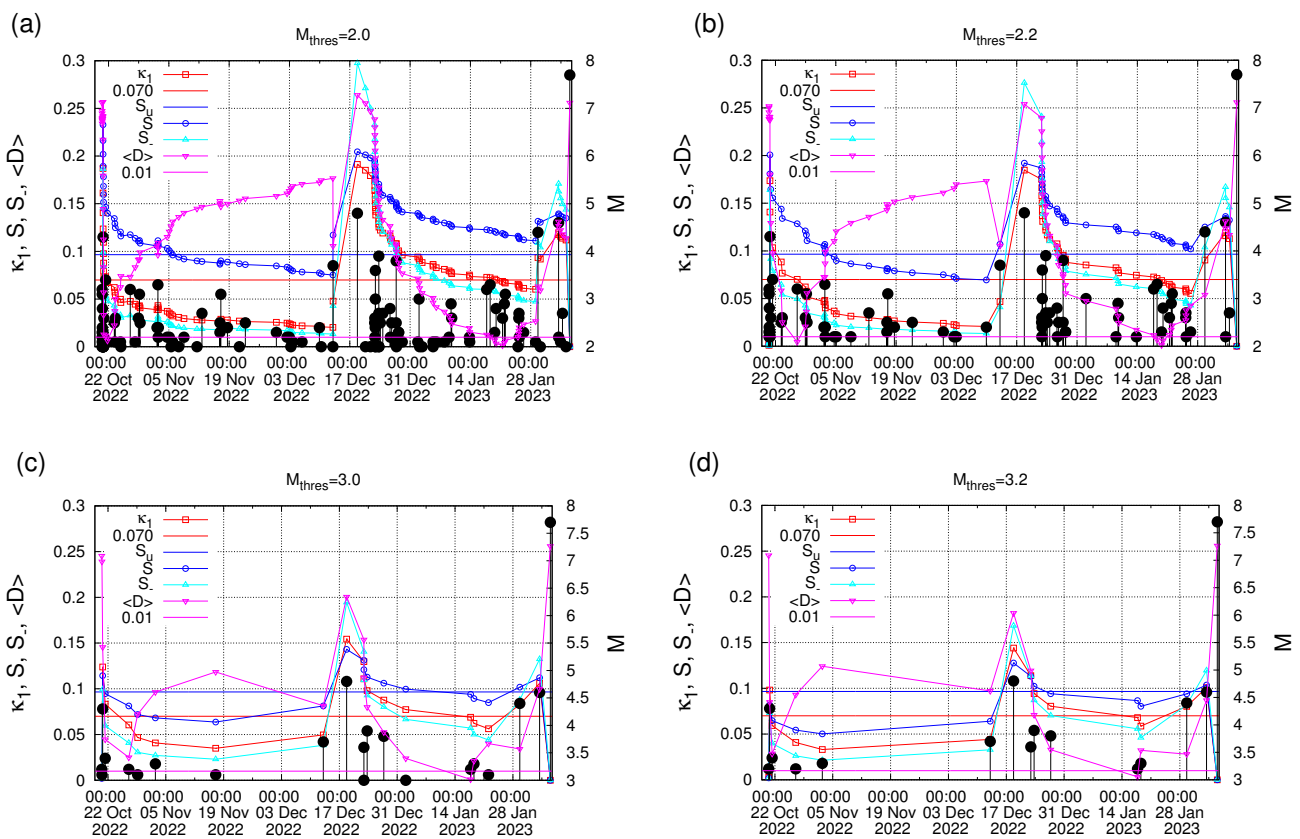

Figure 5. The values of κ_1, S, S_-, and $\langle D \rangle$ (left scale) as they evolve event after event for the seismicity inside the $3° \times 3°$ area around the Kahramanmaraş-Gaziantep $M_w7.8$ Pazarcik EQ epicenter. The EQs reported by AFAD are shown with the black candlesticks ending at circles, the magnitude M of which can be read in the right scale. Panels (**a–d**) correspond to $M_{thres} = 2.0, 2.2, 3.0$, and 3.2, respectively.

Varotsos et al. [5,74] suggested that in order to improve the estimate of the occurrence time of an impending EQ, one should also study the time-series of S_q and ΔS_i of seismicity within the area to suffer the strong EQ, at comparable scales of i consecutive events, in order

to identify similar transient changes. The necessity of such a similarity has been discussed in detail in Section 5 of [74] and mainly stems from the fact that as we approach the strong EQ, fluctuations increase, making their presence evident in both NTA and NESM. The time-series of the Tsallis entropy S_q together with the entropy change ΔS_i in natural time under time reversal are shown in Figure 6 for the time period after the true coincidence (17 to 21 January 2023) until the Kahramanmaraş-Gaziantep $M_w7.8$ Pazarcik EQ. An inspection of Figure 6 reveals a similar transient behavior indicated by the red arrows that lasts from 29 January to 3 February 2023, i.e., almost three days before the Kahramanmaraş-Gaziantep $M_w7.8$ Pazarcik EQ.

We observe that the combination of NTA with NESM may provide an improved estimate of the occurrence time of the Kahramanmaraş-Gaziantep $M_w7.8$ Pazarcik EQ by a significant factor, i.e., from almost two weeks to almost three days. This, i.e., the improvement of the estimate of the occurrence time of an impending strong EQ, is compatible with the results found for the 2011 $M9$ Tohoku, Japan, EQ [5], the 2017 $M8.2$ Chiapas, Mexico, EQ [74], and the 2019 $M7.1$ Ridgecrest EQ [74]. In our view, it is this point that stresses the importance of fluctuations before strong EQs, which should be also studied in the future for other catastrophic EQs.
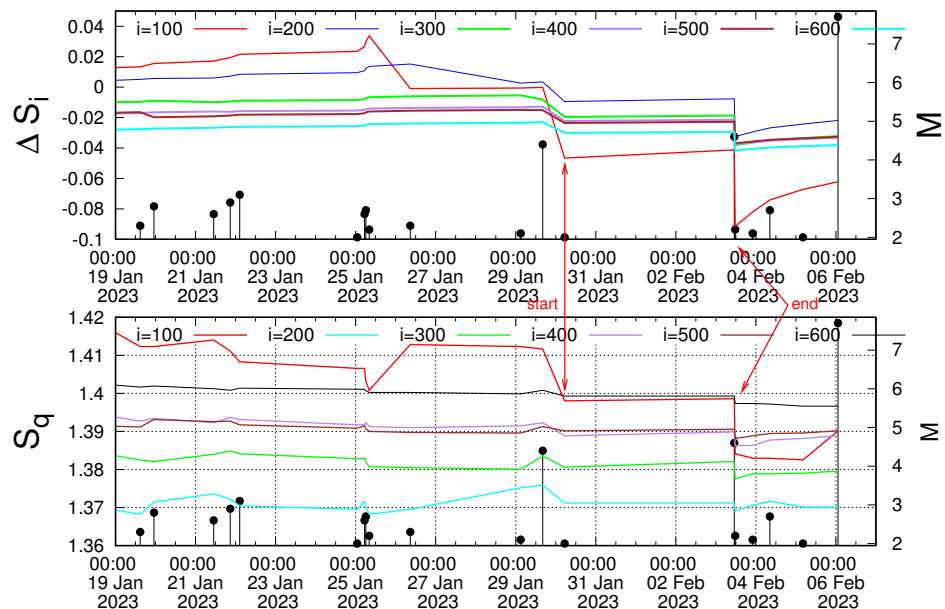
Figure 6. The quantities (upper panel) ΔS_i in NTA and (lower panel) Tsallis entropy S_q of NESM versus the conventional time (UTC) inside the $3° \times 3°$ area around the Kahramanmaraş-Gaziantep $M_w7.8$ Pazarcik EQ epicenter. The red arrows indicate the simultaneous transient changes of ΔS_i and S_q after the validity of the criticality condition $\kappa_1 = 0.070$. They start and end upon the occurrence of two EQs of magnitudes 4.4 and 4.6, respectively. These two EQs occurred on 29 January 2023 at 16:12:39 UTC and on 3 February 2023 at 11:05:08 UTC with epicenters at 35.88° N 35.78° E and 37.21° N 36.40° E, respectively. The EQs reported by AFAD are shown with the black candlesticks ending at circles, the magnitude M of which can be read in the right scale.

As already mentioned, there were no SES data before the Kahramanmaraş, Turkey, EQ doublet. In such cases, NTA may provide an estimate of the epicentral area of the impending EQ by means of a spatiotemporal study, see, e.g., Chapter 3 of [38] and references therein. However, such an analysis is possible when the local EQ catalog used fully covers the study area, which is rarely possible when national boundaries exist in this area. In these cases, our group has suggested [124,125,129] that the average EPS maps based on Equation (15) may provide an estimate of the epicentral location of the impending EQ. The calculation of the ⟨EPS⟩ map should be made on the date of the variability minimum $\beta_{W,min}$ identified before the strong EQ. Following Varotsos et al. [124] and Section 2.6, we depict in Figure 7a

the $\langle EPS \rangle$ map calculated on 18 October 2022. The value of $\langle EPS \rangle$ at the grid point closer to the epicenter of the Kahramanmaraş-Gaziantep $M_w7.8$ Pazarcik EQ is 54%. In Figure 7b, we depict the $\langle EPS \rangle$ map estimated after the last EQ just (12 min) before the $M_w7.5$ Elbistan EQ. Although the $M_w7.8$ took place only 9 h before, EQ nowacasting methodology leads to an $\langle EPS \rangle$ at the grid point closer to the new epicenter of 49%. Interestingly, the two values 54% and 49% compare favorably with the $\langle EPS \rangle$ of 50% that was observed at the grid point closest to the epicenter 38.72° N 43.51° E of the 2011 $M_w7.1$ Van, Turkey, EQ [141] on the date of the corresponding variability minimum; see Table 1 and Section 4 of [124]. The two new $\langle EPS \rangle$ values confirm the original observation [124] that $M \geq 7.1$ EQs usually occur in regions where $\langle EPS \rangle$ is mediocre; see also Figure 6a of [125].
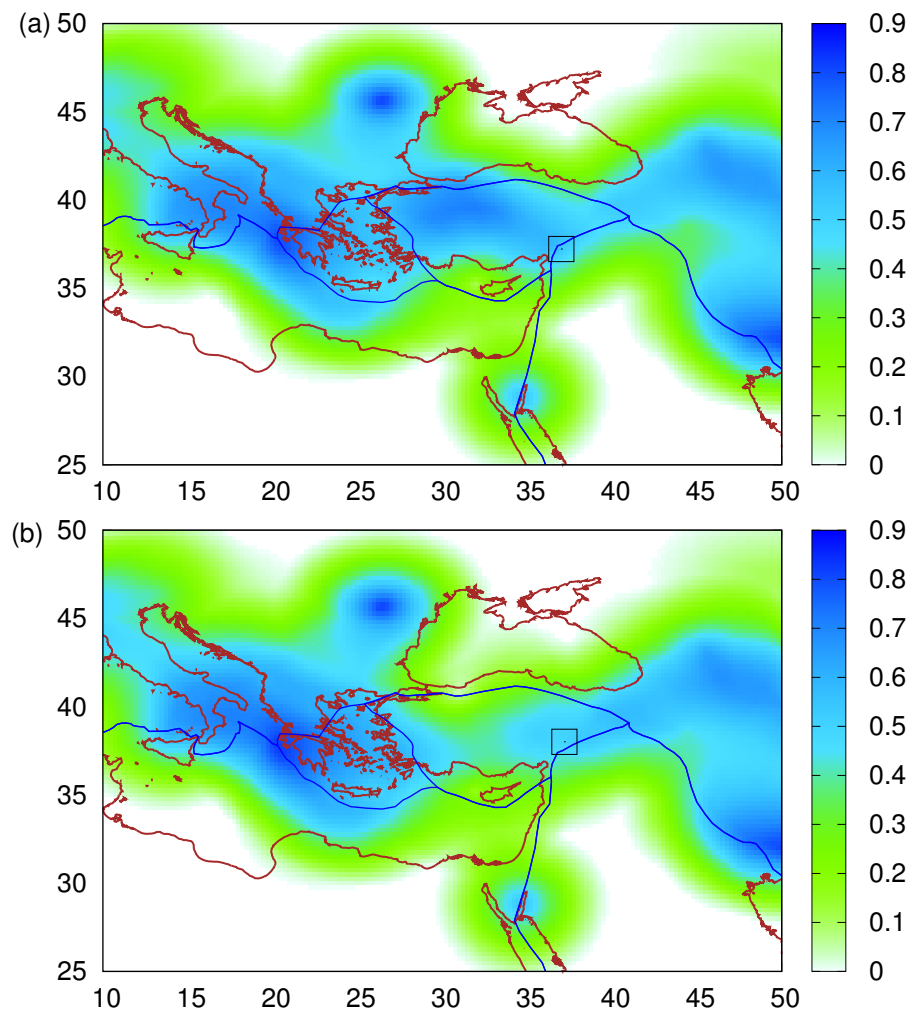
Figure 7. Average EPS maps, depicted by the color scale, according to Equation (15) (see Section 2.6 and [124]) estimated (**a**) on 18 October 2022 for the Kahramanmaraş-Gaziantep $M_w7.8$ Pazarcik EQ and (**b**) on 6 February 2023 at 10:12:17 UTC, i.e., approximately 12 min, before the $M_w7.5$ Elbistan EQ occurrence. The EQ epicenters are shown by the open squares, and the blue thick lines depict the tectonic plate boundaries [19].

4. Summary and Conclusions

We performed NTA of the seismicity preceding the Kahramanmaraş, Turkey, EQ doublet. The following results have been obtained:

1. The study of the fluctuations β_W of the OP of seismicity κ_1 during an almost 20-year period has revealed a unique minimum $\beta_{W,min}$ that ended at 18 October 2022, i.e., almost three and a half months before the Kahramanmaraş-Gaziantep $M_w7.8$ Pazarcik EQ occurrence.

2. The simultaneous study of the DFA exponent a_{300} has also shown a breakdown of the long-range correlations between EQ magnitudes before the $M_w 7.8$ EQ in a way compatible with previous observations in Japan, Mexico, and California.

3. When studying the seismicity after $\beta_{W,min}$ inside a $3° \times 3°$ area around the $M_w 7.8$ EQ epicenter, we found that the power spectrum coincidence of the evolving seismicity to that corresponding to critical behavior $\Pi_{crit}(\omega)$ occurs around 19 January 2023, i.e., almost two weeks before the $M_w 7.8$ EQ occurrence.

4. The above estimation of the occurrence time of the impending strong EQ can be improved when employing NTA and NESM through the comparison of the time-series of the Tsallis entropy S_q and the entropy change ΔS_i under time reversal. Such an analysis reveals that after 3 February 2023 at 11:05:58 UTC, the $M_w 7.8$ EQ was imminent. This result is compatible with those found in Japan, Mexico, and California.

5. By employing the modern method of earthquake nowcasting, we showed how $\langle EPS \rangle$ may provide precursory information on the epicenter location of both the Kahramanmaraş-Gaziantep $M_w 7.8$ Pazarcik EQ and the $M_w 7.5$ Elbistan EQ. The $\langle EPS \rangle$ values were 54% and 49%, respectively, being compatible with previous observations [124,125] that strong EQs occur at locations where $\langle EPS \rangle$ is mediocre.

Interestingly, the first four results are similar to those observed before strong EQs in Japan, Mexico and California, which were mainly subduction or strike–slip EQs. Although every EQ is a different case history, we hope that the present a posteriori results trigger a better understanding of the crustal phenomena as well as shed light in a unified manner on the EQ preparatory processes before strong EQs. Such an approach may become also useful for improving EQ prediction efforts based on NTA and NESM in the future.

Abbreviations

The following abbreviations are used in this manuscript:

AFAD	Turkish Disaster and Emergency Management Authority
DFA	Detrended Fluctuation Analysis
DNA	Deoxyribonucleic Acid
EAF	East Anatolian Fault
EPS	Earthquake Potential Score
EQ	Earthquake
GR	Gutenberg–Richter
NAF	North Anatolian fault
NESM	Non-Extensive Statistical Mechanics
NTA	Natural Time Analysis
OP	Order Parameter
SES	Seismic Electric Signals

USGS	United States Geological Survey
UTC	Universal Time Code
VAN	Varotsos–Alexopoulos–Nomicos

References

1. United States Geological Survey, Earthquake Hazards Program. M 7.8-Pazarcik Earthquake, Kahramanmaras Earthquake Sequence. Available online: https://earthquake.usgs.gov/earthquakes/eventpage/us6000jllz/executive (accessed on 23 November 2023).

2. United States Geological Survey, Earthquake Hazards Program. M 7.5-Elbistan Earthquake, Kahramanmaras Earthquake Sequence. Available online: https://earthquake.usgs.gov/earthquakes/eventpage/us6000jlqa/executive (accessed on 23 November 2023).

3. Jia, Z.; Jin, Z.; Marchandon, M.; Ulrich, T.; Gabriel, A.A.; Fan, W.; Shearer, P.; Zou, X.; Rekoske, J.; Bulut, F.; et al. The complex dynamics of the 2023 Kahramanmaraş, Turkey, M_w 7.8-7.7 earthquake doublet. *Science* **2023**, *381*, 985–990. [CrossRef]

4. International Blue Crescent Relief and Development Foundation. Devastating Earthquakes in Southern Türkiye and Northern Syria, April 6th 2023, Situation Report 20. Available online: https://reliefweb.int/report/turkiye/devastating-earthquakes-southern-turkiye-and-northern-syria-april-6th-2023-situation-report-20-entr (accessed on 23 November 2023).

5. Varotsos, P.; Sarlis, N.; Skordas, E.; Nagao, T.; Kamogawa, M. Natural time analysis together with non-extensive statistical mechanics shorten the time window of the impending 2011 Tohoku M9 earthquake in Japan. *Commun. Nonlinear Sci. Numer. Simul.* **2023**, *125*, 107370. [CrossRef]

6. Tsallis, C. Possible generalization of Boltzmann-Gibbs statistics. *J. Stat. Phys.* **1988**, *52*, 479–487. [CrossRef]

7. Tsallis, C.; Mendes, R.S.; Plastino, A.R. The role of constraints within generalized nonextensive statistics. *Phys. A Stat. Mech. Its Appl.* **1998**, *261*, 534–554. [CrossRef]

8. Gell-Mann, M.; Tsallis, C. *Nonextensive Entropy: Interdisciplinary Applications*; Santa Fe Institute Studies in the Sciences of Complexity; Oxford University Press, Inc.: New York, NY, USA, 2004.

9. Abe, S. Stability of Tsallis entropy and instabilities of Rényi and normalized Tsallis entropies: A basis for q-exponential distributions. *Phys. Rev. E* **2002**, *66*, 046134. [CrossRef]

10. Silva, R.; França, G.S.; Vilar, C.S.; Alcaniz, J.S. Nonextensive models for earthquakes. *Phys. Rev. E* **2006**, *73*, 026102. [CrossRef]

11. Tsallis, C. *Introduction to Nonextensive Statistical Mechanics*; Springer: Berlin, Germany, 2009. [CrossRef]

12. Sarlis, N.V.; Skordas, E.S.; Varotsos, P.A. Nonextensivity and natural time: The case of seismicity. *Phys. Rev. E* **2010**, *82*, 021110. [CrossRef] [PubMed]

13. Telesca, L. A non-extensive approach in investigating the seismicity of L'Aquila area (central Italy), struck by the 6 April 2009 earthquake (M_L = 5.8). *Terra Nova* **2010**, *22*, 87–93. [CrossRef]

14. Telesca, L. Analysis of Italian seismicity by using a non-extensive approach. *Tectonophysics* **2010**, *494*, 155–162. [CrossRef]

15. Telesca, L. Nonextensive analysis of seismic sequences. *Phys. A Stat. Mech. Its Appl.* **2010**, *389*, 1911–1914. [CrossRef]

16. Vallianatos, F.; Michas, G.; Papadakis, G. Non-extensive and natural time analysis of seismicity before the Mw6.4, October 12, 2013 earthquake in the South West segment of the Hellenic Arc. *Phys. A Stat. Mech. Its Appl.* **2014**, *414*, 163–173. [CrossRef]

17. Sotolongo-Costa, O.; Posadas, A. Fragment-Asperity Interaction Model for Earthquakes. *Phys. Rev. Lett.* **2004**, *92*, 048501. [CrossRef] [PubMed]

18. Posadas, A.; Sotolongo-Costa, O. Non-extensive entropy and fragment–asperity interaction model for earthquakes. *Commun. Nonlinear Sci. Numer. Simul.* **2023**, *117*, 106906. [CrossRef]

19. Bird, P. An updated digital model of plate boundaries. *Geochem. Geophys. Geosyst.* **2003**, *4*, 1027. [CrossRef]

20. Varotsos, P.A.; Sarlis, N.V.; Skordas, E.S. Spatio-Temporal complexity aspects on the interrelation between Seismic Electric Signals and Seismicity. *Pract. Athens Acad.* **2001**, *76*, 294–321. http://physlab.phys.uoa.gr/org/pdf/p3.pdf.

21. Papasimakis, N.; Pallikari, F. Correlated and uncorrelated heart rate fluctuations during relaxing visualization. *Europhys. Lett.* **2010**, *90*, 48003. [CrossRef]

22. Varotsos, P.A.; Sarlis, N.V.; Skordas, E.S.; Uyeda, S.; Kamogawa, M. Natural-time analysis of critical phenomena: The case of Seismicity. *Europhys. Lett.* **2010**, *92*, 29002. [CrossRef]

23. Varotsos, P.A.; Sarlis, N.V.; Skordas, E.S. *Natural Time Analysis: The New View of Time*; Precursory Seismic Electric Signals, Earthquakes and other Complex Time-Series; Springer: Berlin/Heidelberg, Germany, 2011. [CrossRef]

24. Vallianatos, F.; Michas, G.; Benson, P.; Sammonds, P. Natural time analysis of critical phenomena: The case of acoustic emissions in triaxially deformed Etna basalt. *Phys. A Stat. Mech. Its Appl.* **2013**, *392*, 5172–5178. [CrossRef]

25. Potirakis, S.M.; Karadimitrakis, A.; Eftaxias, K. Natural time analysis of critical phenomena: The case of pre-fracture electromagnetic emissions. *Chaos* **2013**, *23*, 023117. [CrossRef]

26. Vallianatos, F.; Karakostas, V.; Papadimitriou, E. A Non-Extensive Statistical Physics View in the Spatiotemporal Properties of the 2003 (Mw6.2) Lefkada, Ionian Island Greece, Aftershock Sequence. *Pure Appl. Geophys.* **2014**, *171*, 1343–1354. [CrossRef]

27. Vallianatos, F.; Michas, G.; Hloupis, G. Multiresolution wavelets and natural time analysis before the January-February 2014 Cephalonia (Mw6.1-6.0) sequence of strong earthquake events. *Phys. Chem. Earth Parts A/B/C* **2015**, *85–86*, 201–209. [CrossRef]

28. Hayakawa, M.; Schekotov, A.; Potirakis, S.; Eftaxias, K. Criticality features in ULF magnetic fields prior to the 2011 Tohoku earthquake. *Proc. Jpn. Acad. Ser. B Phys. Biol. Sci.* **2015**, *91*, 25–30. [CrossRef]

29. Pasari, S. Nowcasting Earthquakes in the Bay of Bengal Region. *Pure Appl. Geophys.* **2019**, *176*, 1417–1432. [CrossRef]

30. Yang, S.S.; Potirakis, S.M.; Sasmal, S.; Hayakawa, M. Natural Time Analysis of Global Navigation Satellite System Surface Deformation: The Case of the 2016 Kumamoto Earthquakes. *Entropy* **2020**, *22*, 674. [CrossRef]

31. Vallianatos, F.; Michas, G.; Hloupis, G.; Chatzopoulos, G. The Evolution of Preseismic Patterns Related to the Central Crete (Mw6.0) Strong Earthquake on 27 September 2021 Revealed by Multiresolution Wavelets and Natural Time Analysis. *Geosciences* **2022**, *12*, 33. [CrossRef]

32. Pasari, S.; Verma, H.; Sharma, Y.; Choudhary, N. Spatial distribution of seismic cycle progression in northeast India and Bangladesh regions inferred from natural time analysis. *Acta Geophys.* **2023**, *71*, 89–100. [CrossRef]

33. Varotsos, C.A.; Tzanis, C. A new tool for the study of the ozone hole dynamics over Antarctica. *Atmos. Environ.* **2012**, *47*, 428–434. [CrossRef]

34. Varotsos, C.A.; Tzanis, C.; Cracknell, A.P. Precursory signals of the major El Niño Southern Oscillation events. *Theor. Appl. Climatol.* **2016**, *124*, 903–912. [CrossRef]

35. Varotsos, C.; Efstathiou, M.; Christodoulakis, J. The lesson learned from the unprecedented ozone hole in the Arctic in 2020; A novel nowcasting tool for such extreme events. *J. Atmos.-Sol.-Terr. Phys.* **2020**, *207*, 105330. [CrossRef]

36. Varotsos, C.A.; Mazei, Y.; Saldaev, D.; Efstathiou, M.; Voronova, T.; Xue, Y. Nowcasting of air pollution episodes in megacities: A case study for Athens, Greece. *Atmos. Pollut. Res.* **2021**, *12*, 101099. [CrossRef]

37. Mintzelas, A.; Kiriakopoulos, K. Natural time analysis in financial markets. *Algorithmic Financ.* **2016**, *5*, 37–46. [CrossRef]

38. Varotsos, P.A.; Sarlis, N.V.; Skordas, E.S. *Natural Time Analysis: The New View of Time, Part II. Advances in Disaster Prediction Using Complex Systems*; Springer Nature Switzerland AG: Cham, Switzerland. 2023. [CrossRef]

39. Varotsos, P.; Alexopoulos, K.; Nomicos, K.; Lazaridou, M. Earthquake prediction and electric signals. *Nature* **1986**, *322*, 120. [CrossRef]

40. Varotsos, P.; Lazaridou, M. Latest aspects of earthquake prediction in Greece based on Seismic Electric Signals. *Tectonophysics* **1991**, *188*, 321–347. [CrossRef]

41. Varotsos, P.; Alexopoulos, K.; Lazaridou, M. Latest aspects of earthquake prediction in Greece based on Seismic Electric Signals, II. *Tectonophysics* **1993**, *224*, 1–37. [CrossRef]

42. Varotsos, P. *The Physics of Seismic Electric Signals*; TERRAPUB: Tokyo, Japan, 2005; p. 338.

43. Lazaridou-Varotsos, M.S. *Earthquake Prediction by Seismic Electric Signals. The Success of the VAN Method over Thirty Years*; Springer: Berlin/Heidelberg, Germany, 2013. [CrossRef]

44. Uyeda, S.; Kamogawa, M. The Prediction of Two Large Earthquakes in Greece. *Eos Trans. AGU* **2008**, *89*, 363. [CrossRef]

45. Huang, Q. Rethinking earthquake-related DC-ULF electromagnetic phenomena: Towards a physics-based approach. *Nat. Hazards Earth Syst. Sci.* **2011**, *11*, 2941–2949. [CrossRef]

46. Huang, Q. Retrospective investigation of geophysical data possibly associated with the Ms8.0 Wenchuan earthquake in Sichuan, China. *J. Asian Earth Sci.* **2011**, *41*, 421–427. [CrossRef]

47. Xu, G.; Han, P.; Huang, Q.; Hattori, K.; Febriani, F.; Yamaguchi, H. Anomalous behaviors of geomagnetic diurnal variations prior to the 2011 off the Pacific coast of Tohoku earthquake (Mw9.0). *J. Asian Earth Sci.* **2013**, *77*, 59–65. [CrossRef]

48. Skordas, E.; Sarlis, N. On the anomalous changes of seismicity and geomagnetic field prior to the 2011 9.0 Tohoku earthquake. *J. Asian Earth Sci.* **2014**, *80*, 161–164. [CrossRef]

49. Han, P.; Hattori, K.; Xu, G.; Ashida, R.; Chen, C.H.; Febriani, F.; Yamaguchi, H. Further investigations of geomagnetic diurnal variations associated with the 2011 off the Pacific coast of Tohoku earthquake (Mw 9.0). *J. Asian Earth Sci.* **2015**, *114*, 321–326. [CrossRef]

50. Han, P.; Hattori, K.; Huang, Q.; Hirooka, S.; Yoshino, C. Spatiotemporal characteristics of the geomagnetic diurnal variation anomalies prior to the 2011 Tohoku earthquake (Mw 9.0) and the possible coupling of multiple pre-earthquake phenomena. *J. Asian Earth Sci.* **2016**, *129*, 13–21. [CrossRef]

51. Varotsos, P.A.; Sarlis, N.V.; Skordas, E.S. Identifying the occurrence time of an impending major earthquake: A review. *Earthq. Sci.* **2017**, *30*, 209–218. [CrossRef]

52. Xue, J.; Huang, Q.; Wu, S.; Nagao, T. LSTM-Autoencoder Network for the Detection of Seismic Electric Signals. *IEEE Trans. Geosci. Remote Sens.* **2022**, *60*, 5917012. [CrossRef]

53. Sindirgi, P. A Closed-Form Alternative for the Frequency Distribution of Stably Distributed Random Components in Daily-Mean Self-Potential (SP) Time Series: Example from Urla Station, Turkey. *Pure Appl. Geophys.* **2023**, *180*, 2827–2840. [CrossRef]

54. Varotsos, P.A.; Sarlis, N.V.; Skordas, E.S. Attempt to distinguish electric signals of a dichotomous nature. *Phys. Rev. E* **2003**, *68*, 031106. [CrossRef]

55. Uyeda, S.; Kamogawa, M.; Tanaka, H. Analysis of electrical activity and seismicity in the natural time domain for the volcanic-seismic swarm activity in 2000 in the Izu Island region, Japan. *J. Geophys. Res.* **2009**, *114*, B02310. [CrossRef]

56. Uyeda, S.; Kamogawa, M. Reply to Comment on "The Prediction of Two Large Earthquakes in Greece". *Eos Trans. AGU* **2010**, *91*, 163. [CrossRef]

57. Petrillo, G.; Zhuang, J. The debate on the earthquake magnitude correlations: A meta-analysis. *Sci. Rep.* **2022**, *12*, 20683. [CrossRef]

58. Rundle, J.B.; Turcotte, D.L.; Donnellan, A.; Grant Ludwig, L.; Luginbuhl, M.; Gong, G. Nowcasting earthquakes. *Earth Space Sci.* **2016**, *3*, 480–486. [CrossRef]

59. Rundle, J.B.; Luginbuhl, M.; Giguere, A.; Turcotte, D.L. Natural Time, Nowcasting and the Physics of Earthquakes: Estimation of Seismic Risk to Global Megacities. *Pure Appl. Geophys.* **2018**, *175*, 647–660. [CrossRef]
60. Luginbuhl, M.; Rundle, J.B.; Hawkins, A.; Turcotte, D.L. Nowcasting Earthquakes: A Comparison of Induced Earthquakes in Oklahoma and at the Geysers, California. *Pure Appl. Geophys.* **2018**, *175*, 49–65. [CrossRef]
61. Luginbuhl, M.; Rundle, J.B.; Turcotte, D.L. Natural Time and Nowcasting Earthquakes: Are Large Global Earthquakes Temporally Clustered? *Pure Appl. Geophys.* **2018**, *175*, 661–670. [CrossRef]
62. Luginbuhl, M.; Rundle, J.B.; Turcotte, D.L. Statistical physics models for aftershocks and induced seismicity. *Phil. Trans. R. Soc. A* **2018**, *377*, 20170397. [CrossRef]
63. Rundle, J.; Stein, S.; Donnellan, A.; Turcotte, D.L.; Klein, W.; Saylor, C. The Complex Dynamics of Earthquake Fault Systems: New Approaches to Forecasting and Nowcasting of Earthquakes. *Rep. Prog. Phys.* **2021**, *84*, 076801. [CrossRef]
64. Rundle, J.B.; Donnellan, A.; Fox, G.; Crutchfield, J.P. Nowcasting Earthquakes by Visualizing the Earthquake Cycle with Machine Learning: A Comparison of Two Methods. *Surv. Geophys.* **2022**, *43*, 483–501. [CrossRef]
65. Rundle, J.B.; Donnellan, A.; Fox, G.; Crutchfield, J.P.; Granat, R. Nowcasting Earthquakes:Imaging the Earthquake Cycle in California with Machine Learning. *Earth Space Sci.* **2021**, *8*, e2021EA001757. [CrossRef]
66. Rundle, J.; Donnellan, A.; Fox, G.; Ludwig, L.; Crutchfield, J. Does the Catalog of California Earthquakes, with Aftershocks Included, Contain Information about Future Large Earthquakes? *Earth Space Sci.* **2023**, *10*, e2022EA002521. [CrossRef]
67. Telesca, L.; Lapenna, V.; Macchiato, M. Mono- and multi-fractal investigation of scaling properties in temporal patterns of seismic sequences. *Chaos Solitons Fractals* **2004**, *19*, 1–15. [CrossRef]
68. Telesca, L.; Lapenna, V. Measuring multifractality in seismic sequences. *Tectonophysics* **2006**, *423*, 115–123. [CrossRef]
69. Telesca, L.; Thai, A.T.; Cao, D.T.; Cao, D.T.; Dinh, Q.V.; Mai, X.B. Fractal and Spectral Analysis of Seismicity in the Lai Chau Area (Vietnam). *Fractal Fract.* **2023**, *7*, 776. [CrossRef]
70. Telesca, L.; Thai, A.T.; Lovallo, M.; Cao, D.T.; Nguyen, L.M. Shannon Entropy Analysis of Reservoir-Triggered Seismicity at Song Tranh 2 Hydropower Plant, Vietnam. *Appl. Sci.* **2022**, *12*, 8873. [CrossRef]
71. Zaccagnino, D.; Telesca, L.; Tan, O.; Doglioni, C. Clustering Analysis of Seismicity in the Anatolian Region with Implications for Seismic Hazard. *Entropy* **2023**, *25*, 835. [CrossRef]
72. Hamdache, M.; Peláez, J.A.; Gospodinov, D.; Henares, J.; Galindo-Zaldívar, J.; Sanz de Galdeano, C.; Ranguelov, B. Stochastic Modeling of the Al Hoceima (Morocco) Aftershock Sequences of 1994, 2004 and 2016. *Appl. Sci.* **2022**, *12*, 8744. [CrossRef]
73. Hamdache, M.; Henares, J.; Peláez, J.A.; Damerji, Y. Fractal Analysis of Earthquake Sequences in the Ibero-Maghrebian Region. *Pure Appl. Geophys.* **2019**, *176*, 1397–1416. [CrossRef]
74. Varotsos, P.A.; Sarlis, N.V.; Skordas, E.S.; Nagao, T.; Kamogawa, M.; Flores-Márquez, E.L.; Ramírez-Rojas, A.; Perez-Oregon, J. Improving the Estimation of the Occurrence Time of an Impending Major Earthquake Using the Entropy Change of Seismicity in Natural Time Analysis. *Geosciences* **2023**, *13*, 222. [CrossRef]
75. Sarlis, N.V.; Skordas, E.S.; Varotsos, P.A.; Ramírez-Rojas, A.; Flores-Márquez, E.L. Identifying the Occurrence Time of the Deadly Mexico M8.2 Earthquake on 7 September 2017. *Entropy* **2019**, *21*, 301. [CrossRef]
76. Skordas, E.S.; Christopoulos, S.R.G.; Sarlis, N.V. Detrended fluctuation analysis of seismicity and order parameter fluctuations before the M7.1 Ridgecrest earthquake. *Nat. Hazards* **2020**, *100*, 697–711. [CrossRef]
77. Flores-Márquez, E.L.; Ramírez-Rojas, A.; Perez-Oregon, J.; Sarlis, N.V.; Skordas, E.S.; Varotsos, P.A. Natural Time Analysis of Seismicity within the Mexican Flat Slab before the M7.1 Earthquake on 19 September 2017. *Entropy* **2020**, *22*, 730. [CrossRef]
78. Çıvgın, B.; Scordilis, E.M. Investigating the consistency of online earthquake catalogs of Turkey and surroundings. *J. Seismol.* **2019**, *23*, 1255–1278. [CrossRef]
79. Merdasse, M.; Hamdache, M.; Peláez, J.A.; Henares, J.; Medkour, T. Earthquake Magnitude and Frequency Forecasting in Northeastern Algeria using Time Series Analysis. *Appl. Sci.* **2023**, *13*, 1566. [CrossRef]
80. Mignan, A. Functional shape of the earthquake frequency-magnitude distribution and completeness magnitude. *J. Geophys. Res. Solid Earth* **2012**, *117*, B08302. [CrossRef]
81. Gutenberg, B.; Richter, C.F. Frequency of earthquakes in California. *Bull. Seismol. Soc. Am.* **1944**, *34*, 185–188. [CrossRef]
82. Perez-Oregon, J.; Muñoz-Diosdado, A.; Rudolf-Navarro, A.; Guzmán-Sáenz, A.; Angulo-Brown, F. On the possible correlation between the Gutenberg-Richter parameters of the frequency-magnitude relationship. *J. Seismol.* **2018**, *22*, 1025–1035. [CrossRef]
83. Wiemer, S. A Software Package to Analyze Seismicity: ZMAP. *Seismol. Res. Lett.* **2001**, *72*, 373–382. [CrossRef]
84. Marzocchi, W.; Sandri, L. A review and new insights on the estimation of the b-value and its uncertainty. *Ann. Geophys.* **2003**, *46*, 1271–1282. [CrossRef]
85. Godano, C.; Petrillo, G.; Lippiello, E. Evaluating the incompleteness magnitude using an unbiased estimate of the b value. *Geophys. J. Int.* **2023**, *236*, 994–1001. [CrossRef]
86. van der Elst, N.J. B-Positive: A Robust Estimator of Aftershock Magnitude Distribution in Transiently Incomplete Catalogs. *J. Geophys. Res. Solid Earth* **2021**, *126*, e2020JB021027. [CrossRef]
87. Godano, C.; Petrillo, G. Estimating the Completeness Magnitude mc and the b-Values in a Snap. *Earth Space Sci.* **2023**, *10*, e2022EA002540. [CrossRef]
88. Güvercin, S.E.; Karabulut, H.; Konca, A.O.; Doğan, U.; Ergintav, S. Active seismotectonics of the East Anatolian Fault. *Geophys. J. Int.* **2022**, *230*, 50–69. [CrossRef]

89. Medvedeva, A.; Vydrin, D.; Krylov, A.; Shiryborova, A.; Smirnova, D.; Tsukanova, E.; Kânoğlu, U.; Medvedev, I. The Turkish Tsunami of 6 February 2023 in the Northeastern Mediterranean. *Pure Appl. Geophys.* **2023**, *180*, 3177–3193. [CrossRef]

90. Emre, O.; Duman, T.Y.; Özalp, S.; Šaroğlu, F.; Olgun, S.; Elmacl, H.; Čan, T. Active fault database of Turkey. *Bull. Earthq. Eng.* **2018**, *16*, 3229–3275. [CrossRef]

91. Şeşetyan, K.; Stucchi, M.; Castelli, V.; Capera, A.A.G. Kahramanmaraş-Gaziantep Türkiye M7.7 Earthquake, 6 February 2023 (04:17 GMT+03:00) Large Historical Earthquakes of the Earthquake-Affected Region: A Preliminary Report. Boğaziçi University, Kandilli Observatory and Earthquake Research Institute, Department of Earthquake Engineering: Istanbul, Turkey, 2023. Available online: https://eqe.boun.edu.tr/sites/eqe.boun.edu.tr/files/kahramanmaras-gaziantep_earthquake_06-02-2023_large_hist_eqs_v1.pdf (accessed on 5 December 2023).

92. Brillinger, D.R. Time series, point processes, and hybrids. *Can. J. Stat.* **1994**, *22*, 177–206. [CrossRef]

93. Kanamori, H. Quantification of Earthquakes. *Nature* **1978**, *271*, 411–414. [CrossRef]

94. Feller, W. *An Introduction to Probability Theory and Its Applications, Volume II*; Wiley: New York, NY, USA, 1971.

95. Sarlis, N.V.; Varotsos, P.A.; Skordas, E.S. Flux avalanches in $YBa_2Cu_3O_{7-x}$ films and rice piles: Natural time domain analysis. *Phys. Rev. B* **2006**, *73*, 054504. [CrossRef]

96. Sarlis, N.V.; Skordas, E.S.; Varotsos, P.A. Similarity of fluctuations in systems exhibiting Self-Organized Criticality. *Europhys. Lett.* **2011**, *96*, 28006. [CrossRef]

97. Goldenfeld, N. *Lectures on Phase Transitions and the Renormalization Group*; CRC Press, Taylor & Francis Group: Boca Raton, FL, USA, 2018.

98. Holliday, J.R.; Rundle, J.B.; Turcotte, D.L.; Klein, W.; Tiampo, K.F.; Donnellan, A. Space-Time Clustering and Correlations of Major Earthquakes. *Phys. Rev. Lett.* **2006**, *97*, 238501. [CrossRef]

99. Varotsos, P.A.; Sarlis, N.V.; Skordas, E.S.; Lazaridou, M.S. Seismic Electric Signals: An additional fact showing their physical interconnection with seismicity. *Tectonophysics* **2013**, *589*, 116–125. [CrossRef]

100. Lesche, B. Instabilities of Renyi entropies. *J. Stat. Phys.* **1982**, *27*, 419. [CrossRef]

101. Lesche, B. Renyi entropies and observables. *Phys. Rev. E* **2004**, *70*, 017102. [CrossRef]

102. Peng, C.K.; Buldyrev, S.V.; Havlin, S.; Simons, M.; Stanley, H.E.; Goldberger, A.L. Mosaic organization of DNA nucleotides. *Phys. Rev. E* **1994**, *49*, 1685–1689. [CrossRef]

103. Talkner, P.; Weber, R.O. Power spectrum and detrended fluctuation analysis: Application to daily temperatures. *Phys. Rev. E* **2000**, *62*, 150–160. [CrossRef]

104. Audit, B.; Becry, E.; Muzy, G.; Arneodo, A. Wavelet-based estimators of scaling behavior. *IEEE Trans. Inf. Theory* **2002**, *48*, 2938. [CrossRef]

105. Mantegna, R.N.; Buldyrev, S.V.; Goldberger, A.L.; Havlin, S.; Peng, C.K.; Simons, M.; Stanley, H.E. Linguistic Features of Noncoding DNA Sequences. *Phys. Rev. Lett.* **1994**, *73*, 3169–3172. [CrossRef]

106. Buldyrev, S.V.; Goldberger, A.L.; Havlin, S.; Mantegna, R.N.; Matsa, M.E.; Peng, C.K.; Simons, M.; Stanley, H.E. Long-range correlation properties of coding and noncoding DNA sequences: GenBank analysis. *Phys. Rev. E* **1995**, *51*, 5084–5091. [CrossRef] [PubMed]

107. Ivanov, P.C.; Rosenblum, M.G.; Peng, C.K.; Mietus, J.; Havlin, S.; Stanley, H.E.; Goldberger, A.L. Multifractality in human heartbeat dynamics. *Nature* **1999**, *399*, 461. [CrossRef]

108. Havlin, S.; Buldyrev, S.V.; Bunde, A.; Goldberger, A.L.; Ivanov, P.C.; Peng, C.K.; Stanley, H.E. Scaling in nature: From DNA through heartbeats to weather. *Phys. A Stat. Mech. Its Appl.* **1999**, *273*, 46–69. [CrossRef]

109. Stanley, H.E.; Buldyrev, S.V.; Goldberger, A.L.; Havlin, S.; Peng, C.K.; Simons, M. Scaling features of noncoding DNA. *Phys. A Stat. Mech. Its Appl.* **1999**, *273*, 1–18. [CrossRef]

110. Hardstone, R.; Poil, S.S.; Schiavone, G.; Jansen, R.; Nikulin, V.; Mansvelder, H.; Linkenkaer-Hansen, K. Detrended Fluctuation Analysis: A Scale-Free View on Neuronal Oscillations. *Front. Physiol.* **2012**, *3*, 450. [CrossRef]

111. Bunde, A.; Havlin, S.; Kantelhardt, J.W.; Penzel, T.; Peter, J.H.; Voigt, K. Correlated and Uncorrelated Regions in Heart-Rate Fluctuations during Sleep. *Phys. Rev. Lett.* **2000**, *85*, 3736–3739. [CrossRef]

112. Lennartz, S.; Livina, V.N.; Bunde, A.; Havlin, S. Long-term memory in earthquakes and the distribution of interoccurrence times. *Europhys. Lett.* **2008**, *81*, 69001. [CrossRef]

113. Ivanov, P.C.; Nunes Amaral, L.A.; Goldberger, A.L.; Stanley, H.E. Stochastic feedback and the regulation of biological rhythms. *Europhys. Lett.* **1998**, *43*, 363. [CrossRef]

114. Ivanova, K.; Ackerman, T.P.; Clothiaux, E.E.; Ivanov, P.C.; Stanley, H.E.; Ausloos, M. Time correlations and $1/f$ behavior in backscattering radar reflectivity measurements from cirrus cloud ice fluctuations. *J. Geophys. Res. Atmos.* **2003**, *108*, D9. [CrossRef]

115. Varotsos, C.; Kirk-Davidoff, D. Long-memory processes in ozone and temperature variations at the region 60° S-60° N. *Atmos. Chem. Phys.* **2006**, *6*, 4093–4100. [CrossRef]

116. Kantelhardt, J.; Zschiegner, S.A.; Koscienly-Bunde, E.; Bunde, A.; Havlin, S.; Stanley, H.E. Multifractal detrended fluctuation analysis of nonstationary time series. *Phys. A Stat. Mech. Its Appl.* **2002**, *316*, 87–114. [CrossRef]

117. Oświęcimka, P.; Kwapień, J.; Drożdż, S. Wavelet versus detrended fluctuation analysis of multifractal structures. *Phys. Rev. E* **2006**, *74*, 016103. [CrossRef]

118. Ihlen, E. Introduction to Multifractal Detrended Fluctuation Analysis in Matlab. *Front. Physiol.* **2012**, *3*, 141. [CrossRef]

119. Sarlis, N.V.; Skordas, E.S.; Mintzelas, A.; Papadopoulou, K.A. Micro-scale, mid-scale, and macro-scale in global seismicity identified by empirical mode decomposition and their multifractal characteristics. *Sci. Rep.* **2018**, *8*, 9206. [CrossRef]

120. Peng, C.K.; Buldyrev, S.V.; Goldberger, A.L.; Havlin, S.; Mantegna, R.N.; Simons, M.; Stanley, H.E. Statistical properties of DNA sequences. *Phys. A Stat. Mech. Its Appl.* **1995**, *221*, 180–192. [CrossRef]

121. Goldberger, A.L.; Amaral, L.A.N.; Glass, L.; Hausdorff, J.M.; Ivanov, P.C.; Mark, R.G.; Mictus, J.E.; Moody, G.B.; Peng, C.K.; Stanley, H.E. PhysioBank, PhysioToolkit, and PhysioNet - Components of a new research resource for complex physiologic signals. *Circulation* **2000**, *101*, E215. [CrossRef]

122. Pasari, S.; Sharma, Y. Contemporary Earthquake Hazards in the West-Northwest Himalaya: A Statistical Perspective through Natural Times. *Seismol. Res. Lett.* **2020**, *91*, 3358–3369. [CrossRef]

123. Rundle, J.B.; Donnellan, A. Nowcasting Earthquakes in Southern California With Machine Learning: Bursts, Swarms, and Aftershocks May Be Related to Levels of Regional Tectonic Stress. *Earth Space Sci.* **2020**, *7*, e2020EA001097. [CrossRef]

124. Varotsos, P.K.; Perez-Oregon, J.; Skordas, E.S.; Sarlis, N.V. Estimating the epicenter of an impending strong earthquake by combining the seismicity order parameter variability analysis with earthquake networks and nowcasting: Application in Eastern Mediterranean. *Appl. Sci.* **2021**, *11*, 10093. [CrossRef]

125. Perez-Oregon, J.; Varotsos, P.K.; Skordas, E.S.; Sarlis, N.V. Estimating the Epicenter of a Future Strong Earthquake in Southern California, Mexico, and Central America by Means of Natural Time Analysis and Earthquake Nowcasting. *Entropy* **2021**, *23*, 1658. [CrossRef] [PubMed]

126. Pasari, S.; Simanjuntak, A.V.H.; Neha; Sharma, Y. Nowcasting earthquakes in Sulawesi Island, Indonesia. *Geosci. Lett.* **2021**, *8*, 27. [CrossRef]

127. Pasari, S.; Simanjuntak, A.V.H.; Mehta, A.; Neha; Sharma, Y. A synoptic view of the natural time distribution and contemporary earthquake hazards in Sumatra, Indonesia. *Nat. Hazards* **2021**, *108*, 309–321. [CrossRef]

128. Pasari, S.; Simanjuntak, A.V.H.; Mehta, A.; Neha; Sharma, Y. The Current State of Earthquake Potential on Java Island, Indonesia. *Pure Appl. Geophys.* **2021**, *178*, 2789–2806. [CrossRef]

129. Christopoulos, S.R.G.; Varotsos, P.K.; Perez-Oregon, J.; Papadopoulou, K.A.; Skordas, E.S.; Sarlis, N.V. Natural Time Analysis of Global Seismicity. *Appl. Sci.* **2022**, *12*, 7496. [CrossRef]

130. Pasari, S. Nowcasting earthquakes in Iran: A quantitative analysis of earthquake hazards through natural times. *J. Afr. Earth Sci.* **2023**, *198*, 104821. [CrossRef]

131. Perez-Oregon, J.; Angulo-Brown, F.; Sarlis, N.V. Nowcasting Avalanches as Earthquakes and the Predictability of Strong Avalanches in the Olami-Feder-Christensen Model. *Entropy* **2020**, *22*, 1228. [CrossRef]

132. Fildes, R.A.; Turcotte, D.L.; Rundle, J.B. Natural time analysis and nowcasting of quasi-periodic collapse events during the 2018 Kīlauea volcano eruptive sequence. *Earth Space Sci.* **2022**, *9*, e2022EA002266. [CrossRef]

133. Sarlis, N.V.; Skordas, E.S.; Varotsos, P.A.; Nagao, T.; Kamogawa, M.; Tanaka, H.; Uyeda, S. Minimum of the order parameter fluctuations of seismicity before major earthquakes in Japan. *Proc. Natl. Acad. Sci. USA* **2013**, *110*, 13734–13738. [CrossRef]

134. Varotsos, P.A.; Sarlis, N.V.; Skordas, E.S. Study of the temporal correlations in the magnitude time series before major earthquakes in Japan. *J. Geophys. Res. Space Phys.* **2014**, *119*, 9192–9206. [CrossRef]

135. United States Geological Survey, Earthquake Hazards Program. M 7.3-29 km S of Halabja, Iraq. Available online: https://earthquake.usgs.gov/earthquakes/eventpage/us2000bmcg/executive (accessed on 5 December 2023).

136. Mintzelas, A.; Sarlis, N. Minima of the fluctuations of the order parameter of seismicity and earthquake networks based on similar activity patterns. *Phys. A Stat. Mech. Its Appl.* **2019**, *527*, 121293. [CrossRef]

137. Tenenbaum, J.N.; Havlin, S.; Stanley, H.E. Earthquake networks based on similar activity patterns. *Phys. Rev. E* **2012**, *86*, 046107. [CrossRef]

138. Fawcett, T. An introduction to ROC analysis. *Pattern Recogn. Lett.* **2006**, *27*, 861–874. [CrossRef]

139. Donges, J.; Schleussner, C.F.; Siegmund, J.; Donner, R. Event coincidence analysis for quantifying statistical interrelationships between event time series. *Eur. Phys. J. Spec. Top.* **2016**, *225*, 471–487. [CrossRef]

140. Siegmund, J.F.; Siegmund, N.; Donner, R.V. CoinCalc—A new R package for quantifying simultaneities of event series. *Comput. Geosci.* **2017**, *98*, 64–72. [CrossRef]

141. United States Geological Survey, Earthquake Hazards Program. M 7.1-27 km NNE of Van, Turkey. Available online: https://earthquake.usgs.gov/earthquakes/eventpage/usp000j9rr/executive (accessed on 4 December 2023).